JOURNAL OF GEOPHYSICAL RESEARCH, VOL. 99, NO. D10, PAGES 20,847–20,862, OCTOBER 20, 1994

Analysis and comparison of diurnal variations of cloud radiative forcing: Earth Radiation Budget Experiment and International Satellite Cloud Climatology Project results

Yongseung Kim

NASA Goddard Institute for Space Studies and Columbia University, New York

Abstract. Cloud radiative forcing (CRF) is the radiative impact of clouds on the Earth's radiation budget. This study examines the diurnal variations of CRF using the Earth Radiation Budget Experiment (ERBE) monthly hourly flux data and the flux data derived from the International Satellite Cloud Climatology Project (ISCCP) using the Goddard Institute for Space Studies general circulation model radiation code. The results for the months of April, July, and October 1985 and January 1986 are analyzed. We found that, in general, two data sets agreed. For longwave (LW) CRF the diurnal range over land is generally greater than that observed over oceans. For the 4-month averages the ERBE values are 15.8 W m^{-2} and 6.8 W m^{-2} for land and ocean, respectively, compared with the ISCCP calculated values of 18.4 W m^{-2} and 8.0 W m^{-2}, respectively. The land/ocean contrast is largely associated with changes in cloud amount and the temperature difference between surface and cloud top. It would be more important to note that the clear-sky flux (i.e., surface temperature) variabilities are shown to be a major contributor to the large variabilities over land. The maximum diurnal range is found to be in the summer hemisphere, and the minimum values in the winter hemisphere. It is also shown that the daytime maximum and the nighttime minimum are seen over large portions of land, whereas they occur at any local hour over most oceans. For shortwave (SW) CRF the daytime maximum values are about twice as large as monthly averages, and their highest frequency occurs at local noon, indicating that solar insolation is a primary factor for the diurnal variation of SW CRF. However, the comparison of the ERBE data with the ISCCP results demonstrated that the largest differences in the diurnal range and monthly mean of LW CRF were associated with tropical convergence zones, where clear-sky fluxes could be easily biased by persistent cloudiness and the inadequate treatment of the atmospheric water vapor.

1. Introduction

Clouds are an important component affecting the Earth's radiative energy balance both in the longwave (LW) radiation and in the shortwave (SW) radiation. Clouds absorb the thermal infrared radiation emitted from the Earth's surface and reemit the thermal energy to space, while they reflect the incoming solar radiation. Efforts toward evaluating these radiative effects of clouds are therefore crucial to a better understanding of the role of clouds in the Earth's radiation budget. With this in mind we have investigated the diurnal variations of cloud radiative forcing (CRF).

The previous studies [e.g., *Charlock and Ramanathan*, 1985; *Cess and Potter*, 1987; *Ramanathan et al.*, 1989; *Kyle et al.*, 1991] have introduced the concept of CRF in order to consider the impact of clouds on the Earth's radiation budget. These studies have demonstrated that clouds have a net cooling effect on the Earth-atmosphere system [*Ramanathan et al.*, 1989; *Kyle et al.*, 1991]. It was also shown that clouds reduce the seasonal changes in the net radiative heating [*Harrison et al.*, 1990]. However, none of these studies have addressed the diurnal variations of CRF, though changes in cloud cover are linked to the trends in the daily temperature range [*Karl et al.*, 1993].

Paper number 94JD01722.
0148-0227/94/94JD-01722$05.00

As in previous studies, the components of CRF, LW and SW, are defined as

$$\text{LW CRF} = F_{\text{clear}} - F_{\text{total}}$$

$$\text{SW CRF} = Q_{\text{total}} - Q_{\text{clear}}$$

where F and Q denote the emitted LW and net downward SW fluxes at the top of the atmosphere (TOA), respectively. Since clouds regulate the LW and SW radiation fluxes, the concept of CRF will be useful in the representation of the radiative effect of clouds on the Earth-atmosphere system. In fact, LW CRF is considered to be a measure of the greenhouse effect of clouds because it generally has positive values and thus produces a heating of the Earth-atmosphere system; however, SW CRF represents the cooling (solar albedo) effect due to reflection of SW radiation.

The present analysis can be easily performed using the Earth Radiation Budget Experiment (ERBE) data because the ERBE S-4 product provides both clear-sky and total (all-sky) monthly mean fluxes at each local hour. It is, however, important to note that since these ERBE monthly hourly flux data represent the combination of actual observations (nearly four times a day) and the results of a diurnal

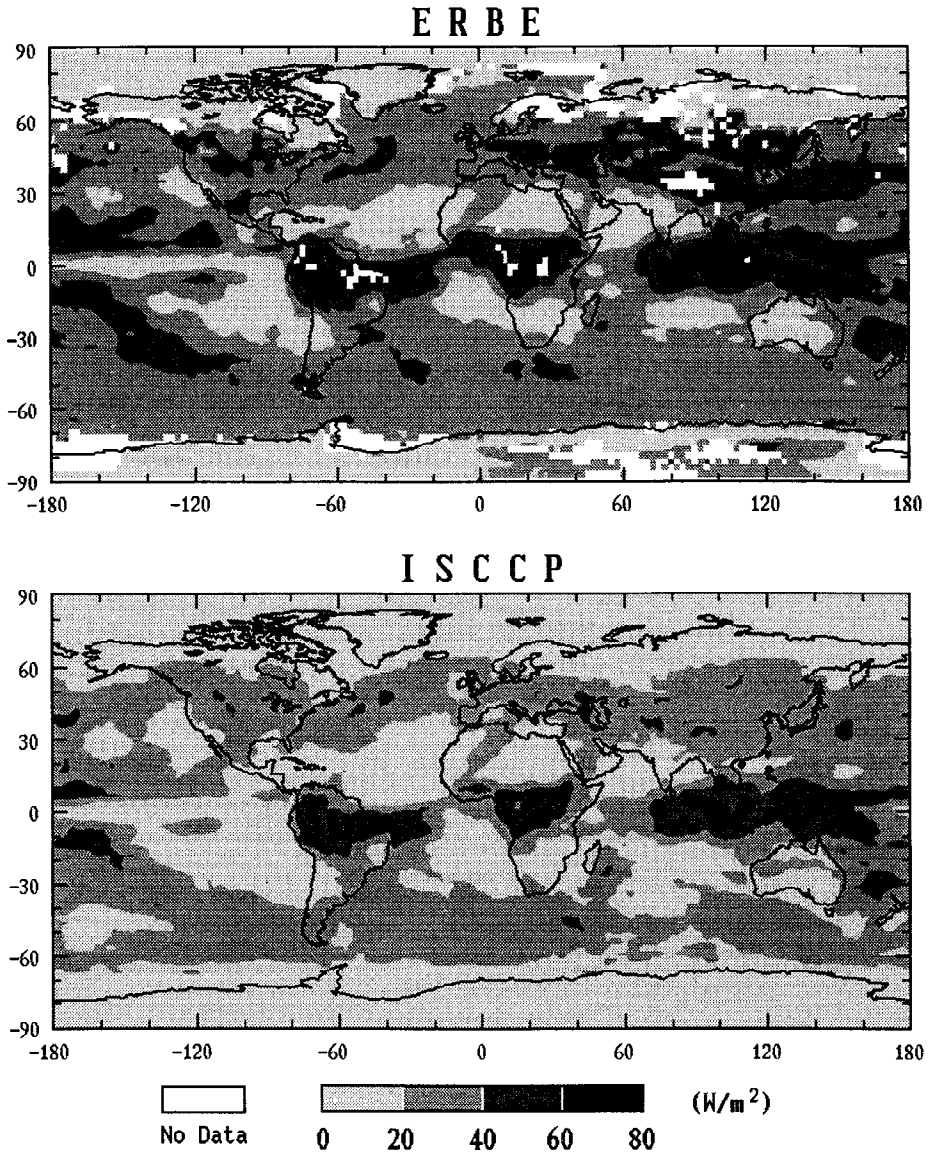

Figure 1. Global distribution of the monthly mean LW CRF (watts per square meter) for (top) ERBE and (bottom) ISCCP for April 1985.

model, there is some concern about their ability to accurately capture the diurnal cycle of CRF. To have a better perspective on this problem, we have supplemented the ERBE data with an examination of the International Satellite Cloud Climatology Project (ISCCP) results.

ISCCP reports the cloud, surface, and atmospheric properties at every 3 hours UT, producing eight measurements a day. These ISCCP C1 data can be used as input to a suitable radiation code to calculate the corresponding radiative fluxes. The radiation code of the Goddard Institute for Space Studies (GISS) general circulation model (GCM) [*Hansen et al.*, 1983] is ideally suited to use the ISCCP cloud property retrievals and ancillary temperature, water vapor, ozone, and surface property data as input to calculate the ISCCP radiative fluxes. Both the ISCCP and the GCM utilize the plane-parallel cloud model comprised of 10-μm Mie scattering spheres, with ISCCP using a lookup table based on doubling method results and the GCM radiation being tuned to reproduce the doubling method cloud albedos as a function of solar zenith angle at visible wavelengths. The GCM framework provides a convenient approach to processing the large volume of data and to properly including the diurnal Sun angle variations as a function of season and latitude and the absorption by atmospheric gases and cloud at infrared wavelengths based on Mie scattering. It is these ISCCP radiative fluxes (Y.-C. Zhang et al., Calculation of surface and top-of-atmosphere radiative fluxes from physical quantities based on International Satellite Cloud Climatology Project data sets, 1, Method and sensitivity to input data uncertainties, submitted to *Journal of Geophysical Research*, 1994) that will be analyzed in this study. Because of their better diurnal sampling the ISCCP radiative fluxes are expected to provide a more accurate representation of diurnal variations.

2. Radiative Flux Data

For the present study we employ two data sets: the ERBE S-4 monthly hourly data and the data (Zhang et al., submit-

ted manuscript, 1994) derived from the GISS GCM radiation code using the ISCCP C1 and C2 data with the ancillary atmosphere/surface data (hereinafter called ISCCP flux data). Here we briefly describe the characteristics of these data sets.

The ERBE data for this study are composed of Earth Radiation Budget Satellite (ERBS) and NOAA 9 scanner measurements. The ERBS is in a precessing orbit with 57° inclination which provides sampling of all local hours every 36 days. NOAA 9 is in a Sun-synchronous orbit with nominal equatorial crossing times at 0230 and 1430 local time. Using the angular directional model, the scanner measurements are converted to instantaneous fluxes at TOA. These measurements are limited to a few times during the day for a given region and consequently require diurnal models for a complete set of monthly hourly data. The diurnal model for SW flux is based on the use of the variation of albedo with solar zenith angle for each scene type [*Brooks et al.*, 1986]. For LW flux the diurnal model over oceans applies linear interpolation between all observed fluxes, while a half-sine model centered about local noon replaces the linear interpolation values over land. The important point is that the ERBE monthly data products are based on observations with limited time sampling, supplemented by diurnal modeling, and considering the differences between the true and the modeled diurnal variations, they may contain biases.

The ISCCP flux data are based on the radiation model calculation as described by Zhang et al. (submitted manuscript, 1994). Radiative flux calculations are performed using the radiative transfer model of the GISS GCM [*Hansen et al.*, 1983], in which observational data sets (the ISCCP C1 and C2 data and the ancillary atmosphere/surface data) replace inputs from other GCM physics subroutines. The use of the ISCCP data has a beneficial effect on the results since, during the period of interest, the ISCCP data are collected from one polar orbiter and five geostationary weather satellites [*Rossow and Schiffer*, 1991] and thus they provide fairly uniform diurnal sampling (temporal sampling every 3 hours) at each location. However, it should be noted that the uncertainties of the ISCCP input data can intrinsically cause

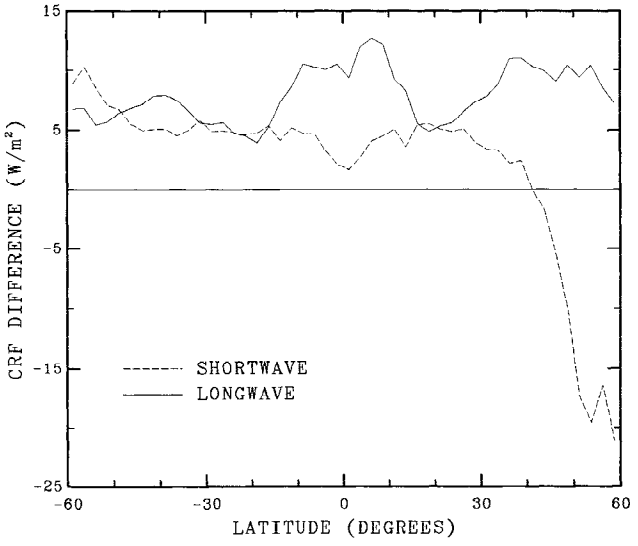

Figure 2. Zonal mean ERBE minus ISCCP CRF differences for April 1985.

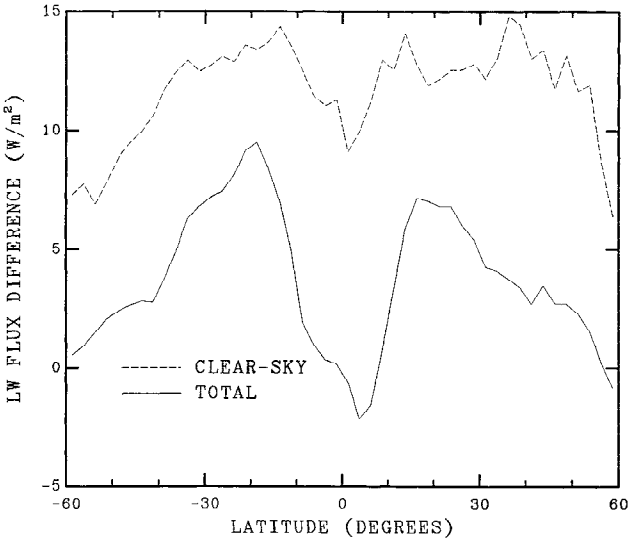

Figure 3. Zonal mean ERBE minus ISCCP LW flux differences for April 1985.

the biases of the calculated radiative fluxes. The results of the sensitivity of input parameters to the individual radiative flux are presented in detail by Zhang et al. (submitted manuscript, 1994), and therefore we will discuss in the following section only some quantities that are relevant to the present study.

The monthly hourly fluxes at TOA are retrieved from two data sets for each 2.5° × 2.5° region. The analyses and comparisons are made for the months of April, July, and October 1985 and January 1986, which we have selected as representative of the seasons in which they fall.

3. Results and Discussion

3.1. Monthly Mean

The global patterns of the monthly mean LW CRF for April 1985 from ERBE and ISCCP are shown in Figure 1. As expected, LW CRF has the maximum values over the tropical convective regions (e.g., Amazon and Congo basins and Indonesia) where optically thick cold clouds significantly reduce the emitted LW radiation. The midlatitude storm tracks are also expected to contribute to a large reduction of LW radiation [*Ramanathan et al.*, 1989]. Desert areas and regions with the persistent low-level clouds are associated with relatively small values of LW CRF because of the low cloud amounts and the reduced effectiveness of the emitted LW absorption from low-level (hence warm) clouds, respectively.

Consistent with the discussion above, both ERBE and ISCCP show the expected regions of maximum and minimum LW CRF. However, this comparison shows that some regional differences in the magnitude of LW CRF exist between the two data sets. For example, over the midlatitude storm tracks and tropical convergence zones, the pattern of the ERBE LW CRF has greater areal coverage with higher values than the ISCCP distribution. One possible explanation for this difference may be the different temporal sampling in the ERBE and ISCCP data products. This is because the accuracy of the monthly mean radiative flux depends upon the diurnal sampling [*Brooks and Minnis*,

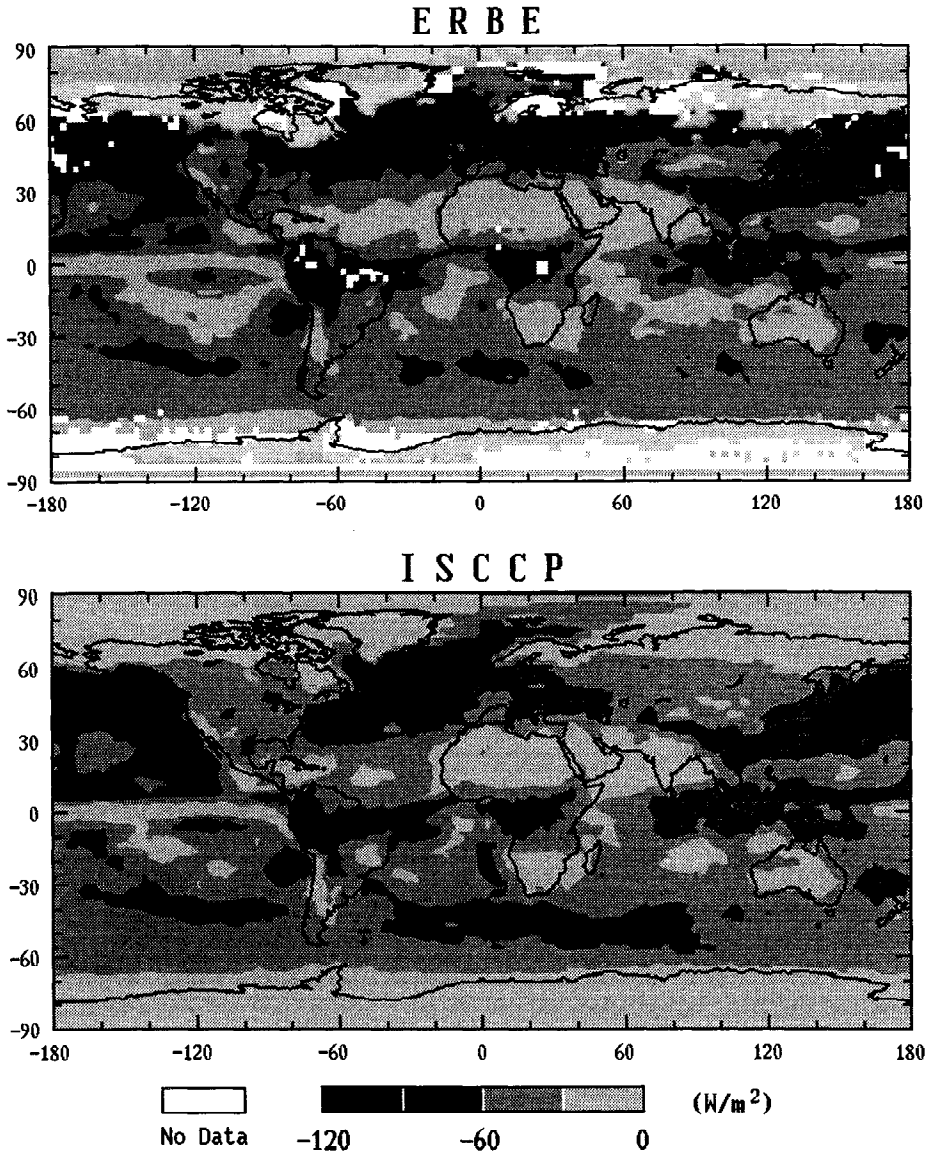

Figure 4. Global distribution of the monthly mean SW CRF (watts per square meter) for (top) ERBE and (bottom) ISCCP for April 1985.

1984; *Rieland and Raschke*, 1991]. These LW CRF differences are also evident in the latitudinal distribution shown in Figure 2, where the SW component is relatively constant with latitude except for the high northern hemisphere (NH) latitudes. Large differences of the LW component are again found over latitudinal belts with persistent clouds. Both LW and SW components show large differences at the NH midlatitudes for which the storm tracks appear to be responsible.

Since CRF is the difference between the clear-sky and the total flux, it is important to examine the CRF differences in terms of these two components. Figure 3 illustrates the zonal mean LW flux differences (ERBE minus ISCCP) for clear-sky and total scenes. Note that the difference in CRF is the area between the two curves. It appears that clouds largely offset the LW flux difference between the two data sets since the total fluxes are in better agreement. The ERBE minus ISCCP clear-sky flux differences are greater than those of total flux, thus producing higher LW CRF for ERBE. Subtropical regions show large LW flux differences for both clear-sky and total, but a compensation between them significantly reduces the LW CRF differences. In the regions with the largest LW CRF differences, such as the tropics (10°S to 10°N) and the midlatitude storm tracks, the clear-sky LW flux differences should account for most LW CRF differences because the clear-sky component is several times greater than the total scene. There may be two aspects of the clear-sky LW flux differences (about 11 W m^{-2} for 4-month average). First is that the ERBE clear-sky LW flux may be overestimated because of the scene identification problems. *Harrison et al.* [1990] reported that the clear-sky LW flux might be overestimated by about 4 W m^{-2}. *Hartmann and Doelling* [1991] demonstrated that the bias could be about 6–7 W m^{-2} over tropical oceans. Moreover, *Stephens and Greenwald* [1991] found that the ERBE clear-sky LW fluxes are systematically higher than the Nimbus 7 counterparts by about 5 W m^{-2} at all latitudes. The second aspect is the biases of the ISCCP clear-sky LW fluxes caused by the

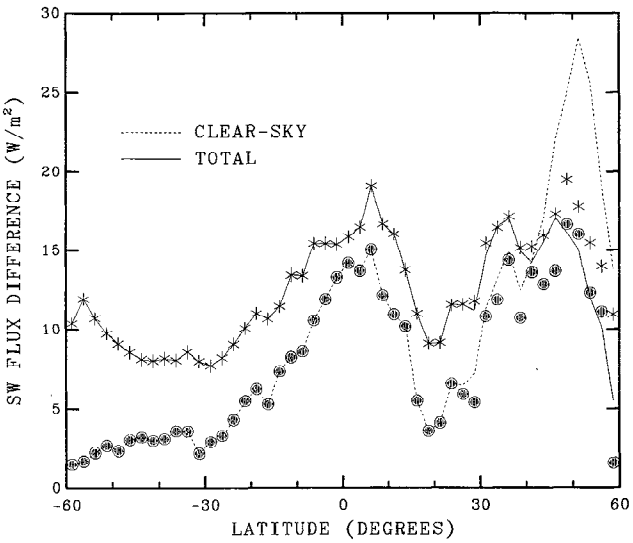

Figure 5. Zonal mean ERBE minus ISCCP net downward SW flux differences for April 1985.

estimated errors in input parameters. It is unlikely that the clear-sky LW flux differences can be produced by a bias of any single parameter from the ISCCP input data as noted by W. B. Rossow and Y.-C. Zhang (Calculation of surface and top-of-atmosphere radiative fluxes from physical quantities based on International Satellite Cloud Climatology Project data sets, 2, Validation and first results, submitted to *Journal of Geophysical Research*, 1994). For example, the use of the estimated TIROS operational vertical sounder (TOVS) errors in water vapor (25%), atmospheric temperature (2 K), and surface temperature (2 K) yields relatively smaller changes in the clear-sky LW fluxes of about 3 W m^{-2}, 5 W m^{-2}, and 2 W m^{-2}, respectively. Also, the ISCCP cloud detection errors can contribute to the clear-sky LW flux differences because the largest change (Zhang et al., submitted manuscript, 1994) was found to be the upward LW flux at surface. Consequently, this large change at surface will lead to the change in the clear-sky LW flux at TOA. If we assume the ISCCP cloud detection errors to be 5% [*Rossow et al.*, 1993], the resultant LW flux change at TOA would be about 6 W m^{-2}. In short, the clear-sky LW flux differences could result from a combination of the above aspects, though the sign of the estimated error in the ISCCP input parameters is uncertain.

Unlike the LW component, the maximum SW CRF for ERBE and ISCCP occurs in the midlatitude oceans of the NH (Figure 4). Cloud systems associated with midlatitude storm tracks and extensive stratus decks over the darker oceans are considered to be largely responsible for this enhanced reflection [*Ramanathan et al.*, 1989]. A secondary peak in SW CRF values occurs over the regions of Indonesia and the Amazon and Congo basins. The geographical patterns show very good agreement between ERBE and ISCCP over most areas. However, the large negative differences are apparent at the high NH latitudes (Figure 2). These large negative differences seem to be associated with the snow- and ice-covered regions, as we will discuss shortly. The components of SW CRF are illustrated in Figure 5 as a means of examining SW CRF differences. The ERBE-absorbed SW fluxes, both clear-sky and total scene, are greater than the ISCCP values. In other words, the ISCCP albedos are higher than the ERBE estimates. An important source for the systematic biases in these SW fluxes would be the differences in the ERBE and ISCCP clear-sky albedos (Rossow and Zhang, submitted manuscript, 1994). Other sources of biases could be possible calibration uncertainties, deficiencies in the GCM spectral integration, or the use of the plane-parallel assumption in the multiple-scattering calculations. An additional feature denoted as solid and dotted lines in Figure 5 is that total differences are larger than those of clear sky except for the regions north of about 41°N where the scene identification algorithms of ERBE and ISCCP are considered less reliable because of the presence of snow and ice. The larger differences in total fluxes consequently lead to the positive SW CRF differences except for the northern latitudes above about 41°N (Figure 2). To demonstrate the contribution of the snow and ice at high latitudes to the absorbed SW flux differences (and thus SW CRF differences), we calculated the zonal averages of these flux differences excluding the snow- and ice-covered grid boxes and presented them in Figure 5 as symbols: hatched circle for clear sky and asterisk for total. The snow and ice cover of the ISCCP C2 data, which was originally obtained from the National Oceanic and Atmospheric Administration/National Environmental Satellite Data and Information Service (NOAA/NESDIS) and NAVY/NOAA Joint Ice Center, was used for this analysis. The resultant flux differences above about 41°N are substantially modified, particularly for clear sky, and have a similar tendency, as shown elsewhere, for total differences to be larger than clear-sky counterparts. This suggests that the negative differences of SW CRF (Figure 2) at high NH latitudes appear to be a consequence of the scene identification problem over the snow- and ice-covered surfaces.

3.2. Diurnal Range

LW components. For the month of April 1985 the global distributions of the diurnal range of LW CRF for ERBE and ISCCP data are illustrated in Figure 6. A notable feature is the land/ocean contrast. The global diurnal range over land is generally greater than that observed over oceans. Note that the 0–20 W m^{-2} range is divided into two bins for better contrast over oceans. The seasonal variations of the diurnal range of LW CRF are summarized in Table 1. As indicated, with the exception of April 1985 for the ISCCP land and ERBE ocean results, the maximum diurnal range is observed in the summer hemisphere and the minimum values in the winter hemisphere. Four-month averages of land and ocean are 15.8 W m^{-2} and 6.8 W m^{-2}, respectively, for ERBE and 18.4 W m^{-2} and 8.0 W m^{-2}, respectively, for ISCCP. The land/ocean contrast for the diurnal range of LW CRF is primarily associated with the diurnal variations of cloud amount and of the surface/cloud top temperature difference. To demonstrate this, we calculated the diurnal range of cloud amount and of the surface minus cloud top temperature using the ISCCP data. Results for April 1985 are shown in Figure 7, and the global estimates for July 1985 and January 1986 are summarized in Table 2. We can clearly see the land/ocean and seasonal difference. Also shown in Table 2 is the diurnal range of surface temperature and the cloud top temperature which can be a measure of the relative contribution of each variable to the diurnal range of the surface/cloud top temperature difference. Changes of two

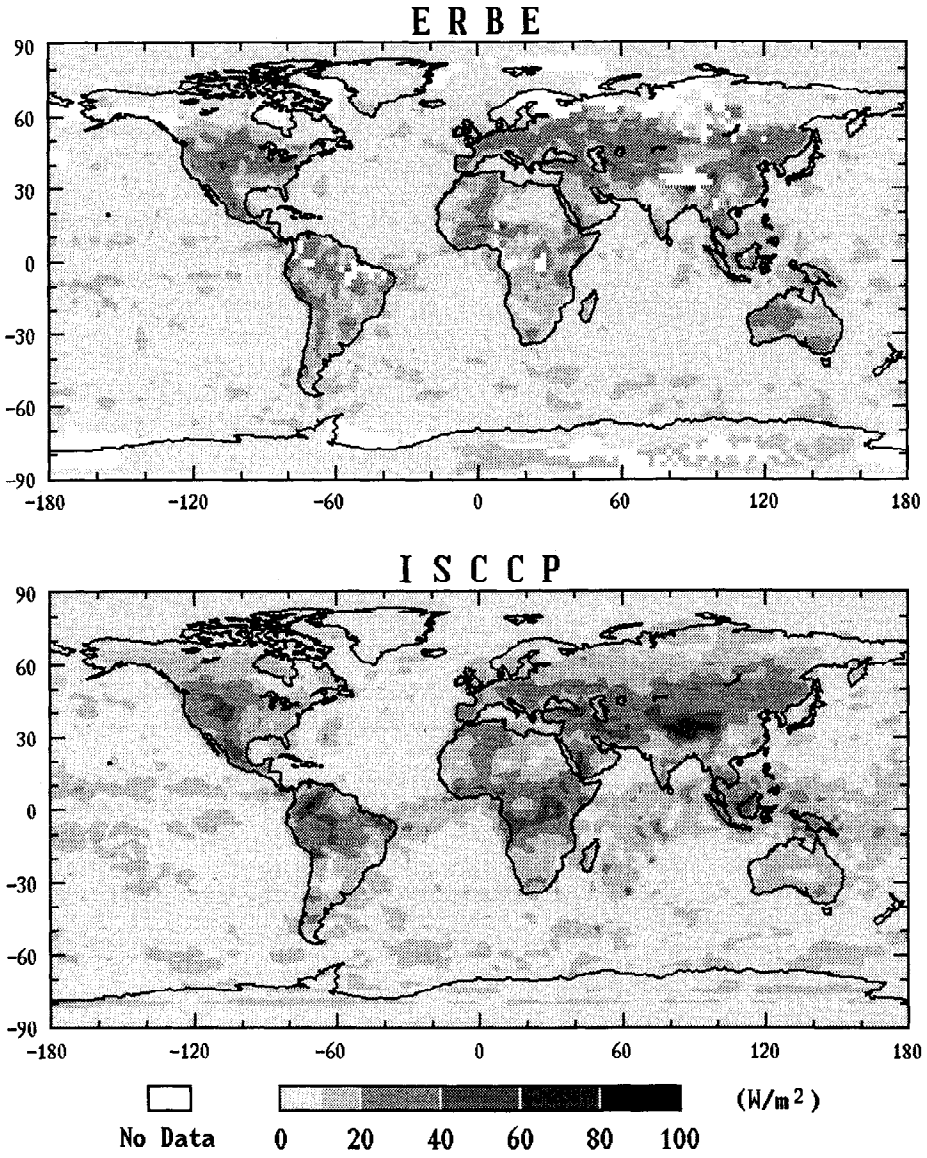

Figure 6. Global distribution of diurnal range of LW CRF for (top) ERBE and (bottom) ISCCP for April 1985.

TABLE 1. Global Estimates of the LW CRF Diurnal Range

	Data Set	Northern Hemisphere		Southern Hemisphere		Global	
		Land	Ocean	Land	Ocean	Land	Ocean
April 1985	ERBE	17.4	6.4	15.3	6.6	16.4	6.5
	ISCCP	23.1	8.2	18.4	8.3	20.8	8.2
July 1985	ERBE	18.4	7.7	11.3	5.9	15.0	6.8
	ISCCP	21.4	8.9	10.6	7.2	16.2	8.1
October 1985	ERBE	14.3	6.9	17.6	6.2	15.9	6.6
	ISCCP	15.0	8.4	22.8	7.3	18.7	7.8
January 1986	ERBE	10.9	6.6	20.9	8.0	15.7	7.3
	ISCCP	9.8	7.3	26.2	8.5	17.7	7.9
4-month averages	ERBE	15.3	6.9	16.3	6.7	15.8	6.8
	ISCCP	17.3	8.2	19.5	7.8	18.4	8.0

Estimates are given in watts per square meter.

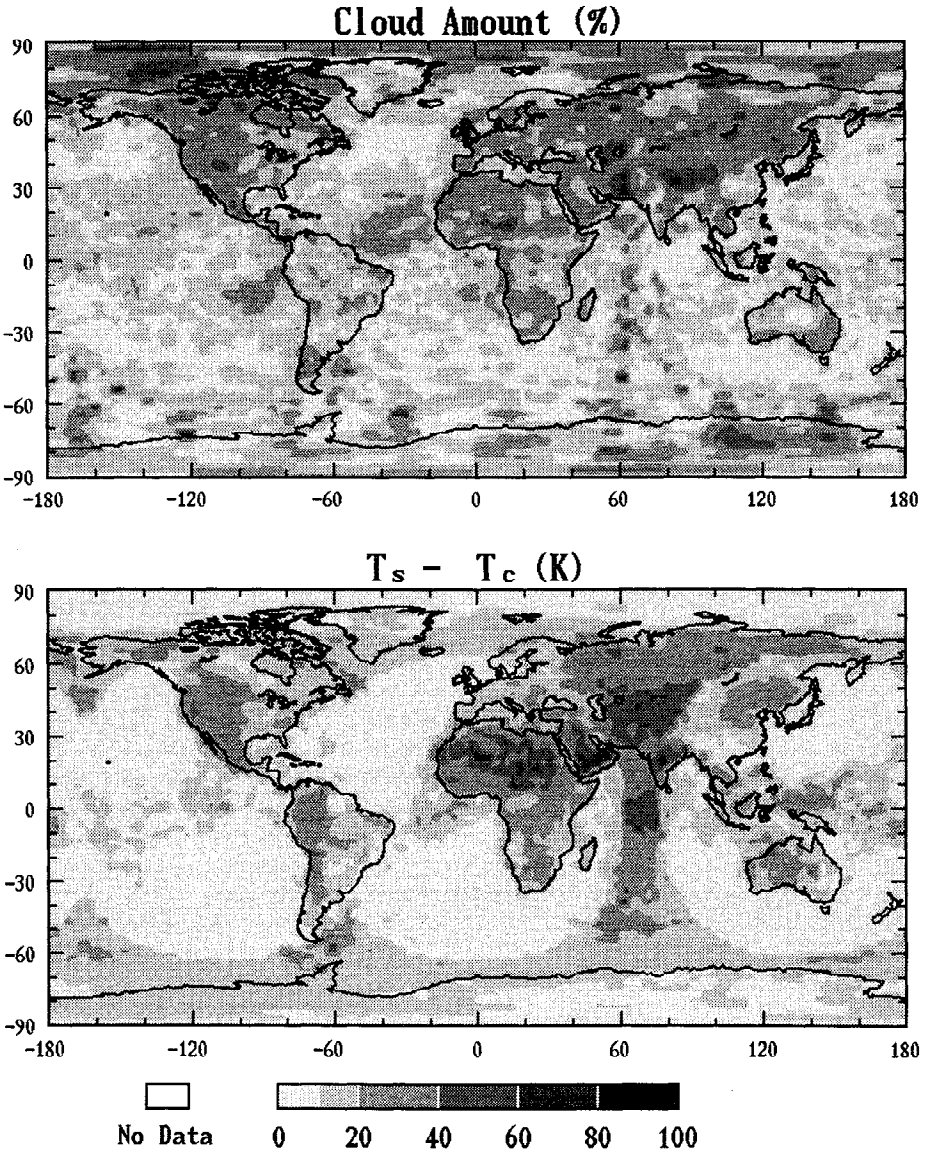

Figure 7. Diurnal range of (top) cloud amount and (bottom) surface minus cloud top temperature for April 1985 from ISCCP C2 data.

TABLE 2. Global Estimates of the Diurnal Range for TCA, TS Minus TC, TS, and TC

		Northern Hemisphere			Southern Hemisphere		
	Parameters	Land	Ocean	Total	Land	Ocean	Total
July 1985	TCA	23.0	13.2	17.6	16.8	12.0	12.7
	TS − TC	22.6	9.0	14.4	15.7	5.2	7.1
	TS	21.5	2.7	10.3	14.8	2.1	4.5
	TC	23.8	8.9	14.7	16.7	5.4	7.4
January 1986	TCA	18.7	12.8	15.6	21.6	14.7	14.9
	TS − TC	18.7	5.5	9.0	23.2	7.2	10.0
	TS	17.8	2.8	7.5	20.5	2.5	5.2
	TC	21.1	5.5	10.0	25.5	7.3	10.3

TCA, TS, and TC represent total cloud amount (percent), surface temperature (kelvins), and cloud top temperature (kelvins), respectively.

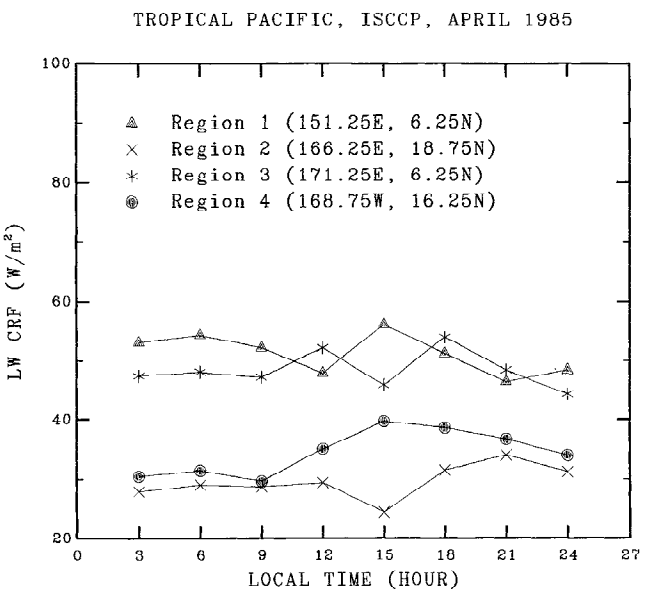

Figure 8. Diurnal variation of LW CRF for four 2.5° × 2.5° regions in the tropical Pacific Ocean.

variables appear to be equally important for a large diurnal range of the surface/cloud top temperature difference over the summer hemisphere land, while the cloud top temperature changes seem to be a major contributor over oceans.

Other than the land/ocean contrast as seen in Figure 6, both ERBE and ISCCP data commonly lack strong diurnal variations over the midlatitude storm tracks where the large monthly mean LW CRF is observed. It appears therefore that the storm tracks in the midlatitudes are effective in reducing the emitted LW radiation but undergo diurnal cycles with relatively small amplitude, or it suggests that these synoptic-scale storms have no preferred diurnal phase. Over oceanic stratus regions (e.g., west coast of South America) the diurnal variations of LW CRF are seen to be small compared to considerable changes in albedo as discussed later in this section. The ISCCP results in Figures 6 and 7 also illustrate some interesting patterns over a band between about 60°E and about 77°E of the Indian Ocean. Relatively large values in this region seem to be caused by undersampling of diurnal cycles as discussed in section 3.4. In addition, we note that the diurnal range of LW CRF over the tropical deep convective oceans is not as large as the land variability. This is apparently consistent with the results of *Hartmann et al.* [1991]. Of particular interest over these tropical oceans is the diurnal cycle of precipitation associated with deep convection. Using precipitation data for the spring season for four small islands, *Gray and Jacobson* [1977] found that the maximum precipitation occurred at about 0600 local time and the minimum value at about 2000 local time. To compare this precipitation behavior with the diurnal phase of LW CRF, we extracted the LW CRF values for four 2.5° × 2.5° regions within which their four island observations were collocated. As shown in Figure 8, none of these LW CRF cycles appear to be consistent with the phase of the precipitation cycle. Since high-level clouds have been used as an important indicator of the tropical deep convection and precipitation [e.g., *Albright et al.*, 1985; *Duvel*, 1989; *Fu et al.*, 1990], we further examined the cloud types (i.e., low, middle, and high) of these regions (not shown) and found that only the phases of regions 1 and 4 were closely related to changes in high-level clouds. In such cases, LW CRF tends to peak at 1500 local time over these regions, consistent with the results of *Albright et al.* [1985] and *Duvel* [1989]. However, the disagreement with surface observations mentioned above remains inexplicable, though there is an implication that further separation of high-level clouds seems necessary for a proper determination of precipitation variability [*Fu et al.*, 1990].

Since LW CRF is the difference between clear-sky and total fluxes, changes in clear-sky fluxes can produce variations in LW CRF without any change in cloud. It is therefore interesting to see to what degree the land/ocean difference described above can be explained by the larger diurnal variation of clear-sky fluxes over land. For this analysis we calculated the diurnal ranges of clear-sky fluxes, total LW fluxes, and LW CRF for 4-month averages. Figure 9 shows the geographical distributions of three variables for the ERBE data (ISCCP results are not shown for simplicity). The LW CRF patterns (Figure 9, top) are analogous to those for the month of April (Figure 6, top) in that they show the land/ocean contrast. As expected, the clear-sky flux variations over land are greater than those observed over oceans. More importantly, there are regions where these clear-sky variations play a dominant role in determining the LW CRF variations. For example, central Europe and southern China exhibit relatively small variations in the total fluxes (Figure 9, bottom) but large variations in clear-sky fluxes (Figure 9, middle) that consequently produce the large diurnal range observed in LW CRF. To further emphasize that the large diurnal variations of LW CRF over land could be associated with the surface change, not exclusively with cloud variations, we tested the sensitivity of changes in total cloud amount, surface temperature, and cloud top temperature to the diurnal range of LW CRF. We calculated the diurnal range of LW CRF for 1 day (eight measurements 3 hours UT apart on July 15, 1985) with input parameter changes using the same GCM radiation code that produced the ISCCP flux data of this study. Results are illustrated in Table 3. For the standard case, there are no changes in ISCCP input parameters. Other control experiments represent the calculations with the daily maximum total cloud amount (TCA), the surface temperature (TS), and the daily minimum cloud top temperature (TC) at given grid boxes while holding other input parameters the same as specified for July 15. Consistent with the monthly results, the standard case shows a large diurnal range over land in the summer hemisphere. A more important point is that the surface temperature is the largest contributor to the diurnal range of LW CRF over land in the summer hemisphere. Therefore, along with the above results, this suggests that the large diurnal variation of LW CRF over land is substantially affected by clear-sky variability (i.e., surface change).

With respect to the difference between ERBE and ISCCP results (Table 1), one can see that in all but the winter hemisphere over land, the ERBE measurements underestimate the diurnal range relative to the ISCCP calculated values. This is an interesting result in view of the situation that the ERBE monthly mean values are higher than the ISCCP estimates. Different diurnal sampling is believed to be an important factor for these differences. The ERBE data used for this study are composed of the two-satellite (ERBS

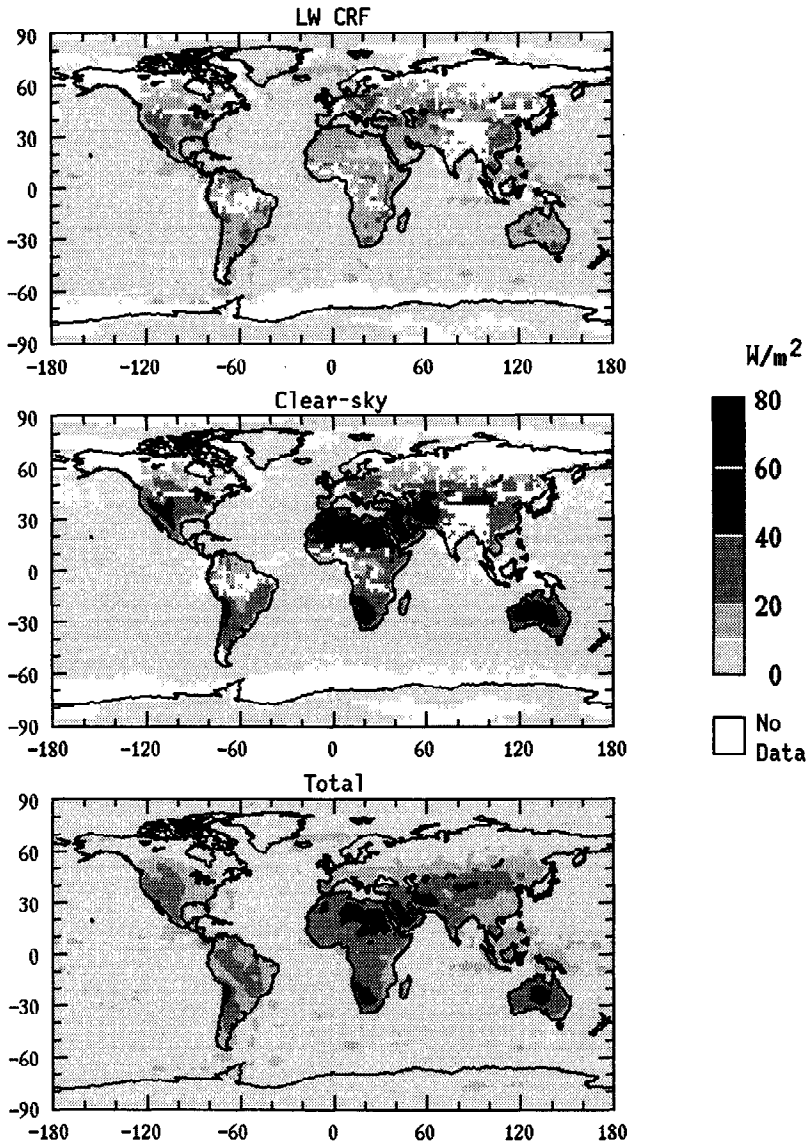

Figure 9. Diurnal range of (top) LW CRF, (middle) clear-sky LW flux, and (bottom) total LW flux for 4-month (April, July, and October 1985 and January 1986) averages from ERBE data.

and NOAA 9) system that produces nearly four actual measurements during the day for a given region. With these observations and the diurnal model the ERBE data processing yields a complete set of the monthly hourly flux data. Therefore the goodness of the diurnal model certainly determines the quality of the monthly hourly data. On the other hand, the ISCCP data are measurements made every 3 hours (eight times a day) and thus have the potential to better capture diurnal components. For example, Figure 10 depicts the diurnal variation of LW CRF for a grid box (108.75°W, 38.75°N) in the Rocky Mountains area where the total cloud amount from the ISCCP data reaches maximum at 1500 local time, solely because of the increase in high-level clouds. It is certainly notable that the phase difference between two data

TABLE 3. Global Estimates of the LW CRF Diurnal Range for July 15, 1985, as Calculated From the GISS GCM Radiation Code

Control Experiment	Northern Hemisphere			Southern Hemisphere		
	Land	Ocean	Total	Land	Ocean	Total
Standard	45.6	29.8	35.7	23.1	26.2	25.4
Maximum TCA	42.0	28.3	33.4	21.3	23.9	23.2
Maximum TS	49.3	30.1	37.1	25.0	26.8	26.2
Minimum TC	46.7	24.7	33.8	28.2	20.9	21.6

Estimates are given in watts per square meter.

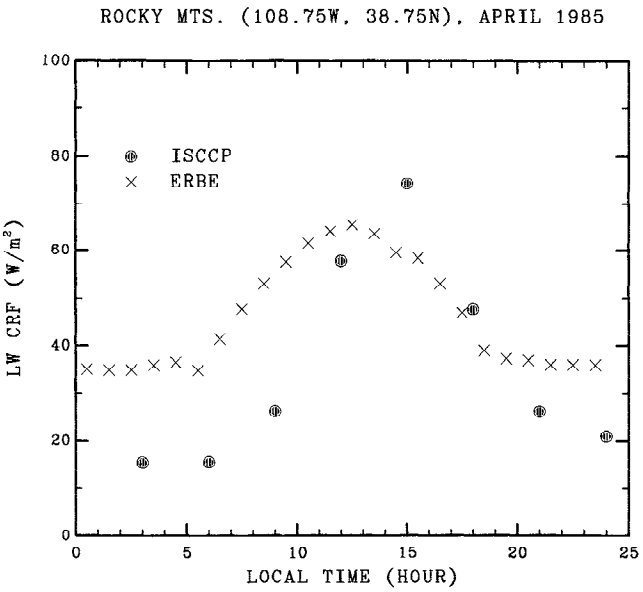

Figure 10. Diurnal variation of LW CRF in the Rocky Mountains (108.75°W, 38.75°N).

sets which is originally caused by diurnal sampling can be important to the difference of the diurnal range. *Cheruy et al.* [1991] pointed out that the incomplete time sampling was one of main reasons for the significant differences for the diurnal cycle of LW radiation. In addition to examining the differences between two data sets, the latitudinal variations of these differences are shown in Figure 11. The largest differences in diurnal ranges are associated with the seasonal movement of tropical convergence zones in which clear-sky fluxes can be easily biased by persistent cloudiness and the inadequate treatment of the atmospheric water vapor.

SW components. Since SW radiation is not available at night, we obtain the maximum SW CRF instead of the diurnal range. Figure 12 illustrates the results and exhibits distributions quite similar to the monthly mean field (Figure 4), except for the magnitude. Because of the strong dependence of SW CRF on insolation [*Harrison et al.*, 1990], this maximum SW CRF is seen to be about twice as large as monthly mean values and tends to occur when the insolation reaches its highest value, as will be shown below.

An important role of clouds in SW radiation is to increase reflection (i.e., albedo) relative to clear sky. Although SW CRF by itself includes albedo change by clouds in terms of differences between clear-sky and total albedos, we do not make any attempt to examine the daytime change of SW CRF because of insolation dependence problems as mentioned above. Alternatively, we present the results of total albedo differences between 0900 and 1500 local time. This approach [e.g., *Hartmann et al.*, 1991] has been used to characterize the diurnal variations of total albedo with clouds since the effect of the solar zenith angle on albedo is symmetric about local noon. Figure 13 shows the global distribution of the 0900 minus 1500 local time total albedo differences of April 1985 for ERBE and ISCCP data. It is not appropriate to interpret the ISCCP results since the ISCCP data is 3 hourly so that the albedo dependence on solar zenith angle seems to significantly affect the patterns. The ERBE results, however, provide some interesting patterns related to the change of cloud types. A notable feature, compared to LW results, is the diurnal change of marine low-level clouds which characterize an increase in cloud amount in the morning and a decrease in the afternoon. The well-known regions of marine low-level clouds such as California coast, the west coasts of South America and South Africa, and the midlatitude oceans in the southern hemisphere are highlighted with a range in total albedo changes of 10–20%, while the differences over most land and oceans range from 0 to 10%. Also, the negative differences of albedos (−5% to 0%) associated with an increase in high-level clouds in the afternoon can be seen over mountain areas such as Tibet and the Rocky Mountains. The albedo changes at high latitudes are uncertain because of scene identification difficulties between the clouds and the underlying surface (snow and ice).

3.3. Times of Maximum and Minimum CRF

Illustrated in Figure 14 are the local times of maximum and minimum LW CRF for 4-month averages. For a better comparison with the ISCCP results, the ERBE data were sorted into 3-hour bins; for example, the frequency at 0300 local time represents a sum of quantities at 0200, 0300, and 0400 local time. While there exists general agreement between the ISCCP and the ERBE results in terms of diurnal phase, significant differences exist in the diurnal distribution of LW CRF. Some of these differences may be attributable to the characteristics of the individual flux data sets. For example, the temporal sampling of the ISCCP data is 3 hourly, and thus the ISCCP calculated fluxes can only resolve the time of maximum or minimum LW CRF to within 3 hours. The ERBE data, on the other hand, have a 1-hour interval but may contain biases due to their use of diurnal model results. Nevertheless, both data sets agree that the maximum LW CRF occurs during the daytime over land (nighttime minimum) and at any local hour over oceans.

The diurnal variability of LW CRF over land reflects both the diurnal cycle of the cloud amount and the diurnal cycle of the temperature difference between the surface and the cloud top. The maxima in both of these quantities, as

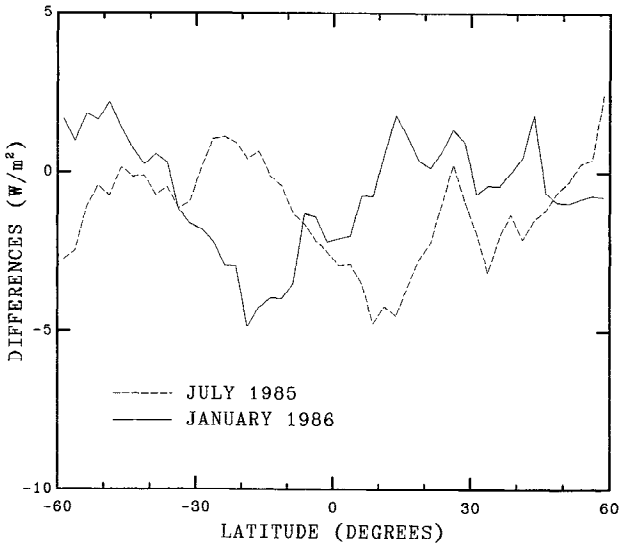

Figure 11. Zonal mean ERBE minus ISCCP LW CRF diurnal range differences for July 1985 and January 1986.

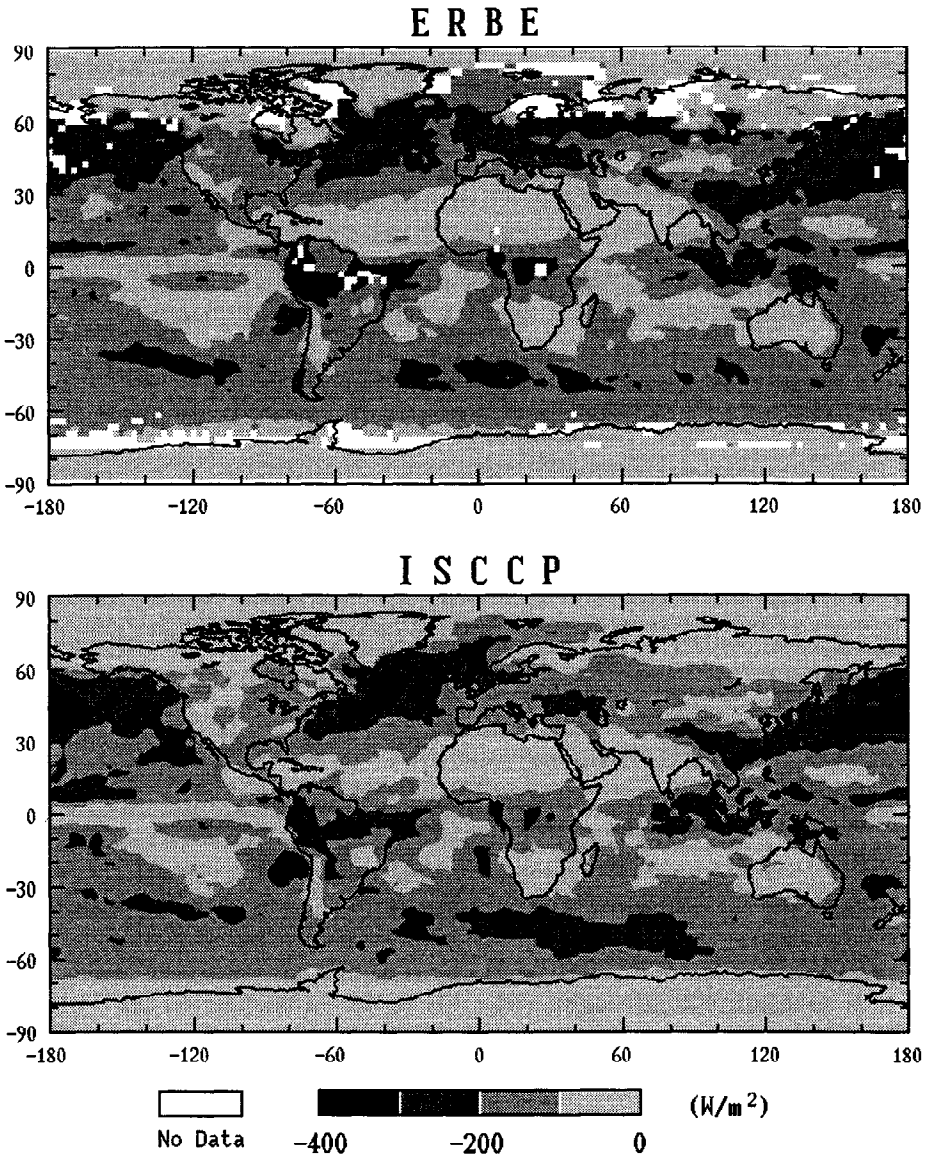

Figure 12. Daytime maximum SW CRF (watts per square meter) for (top) ERBE and (bottom) ISCCP for April 1985.

inferred from the ISCCP data, and the maximum in LW CRF all occur at 1500 local time. The minimum in LW CRF corresponds more closely to the minimum in cloud amount and low surface minus cloud top temperature difference.

It is interesting to note that the daytime maximum LW CRF over land for the ERBE data tends to be earlier than that of the ISCCP. This is because the ERBE flux data over land use the half-sine model that is symmetrical about local noon and would thus be biased toward noon [*Harrison et al.*, 1988]. Furthermore, we have calculated the annual averages of the ERBE data for this analysis and found results similar to those in the above discussion.

For the SW component the times of maximum values are depicted in Figure 15. The unique feature common in both data is that the highest frequency occurs at the solar noon and is out of phase with maximum cloud amount. This result indicates that SW CRF depends strongly on solar insolation, consistent with the results of *Harrison et al.* [1990]. We note some interesting high-latitude variabilities that arise from the extended daylight hours during these months.

3.4. Significance Test for Diurnal Variability

In this section we examine the statistical significance of monthly hourly averages for the diurnal variation. If the diurnal sampling is inappropriate, the diurnal variation for a given region using the monthly hourly data may or may not be statistically significant. Such a test can be carried out using the Fisher F test suggested by *Kandel* [1983] and *Brooks et al.* [1986]. In this application the ISCCP daily hourly flux data (8 hours × 30 days) have been used because the ERBE statistics are not available, though the test for the ERBE data is considered to be more requisite. We present the result of LW CRF for the month of April 1985 in Figure 16, where F values greater than about 95% significance level are stippled. The distribution is quite similar to that of the diurnal range of LW CRF (Figure 6, bottom). It is evident

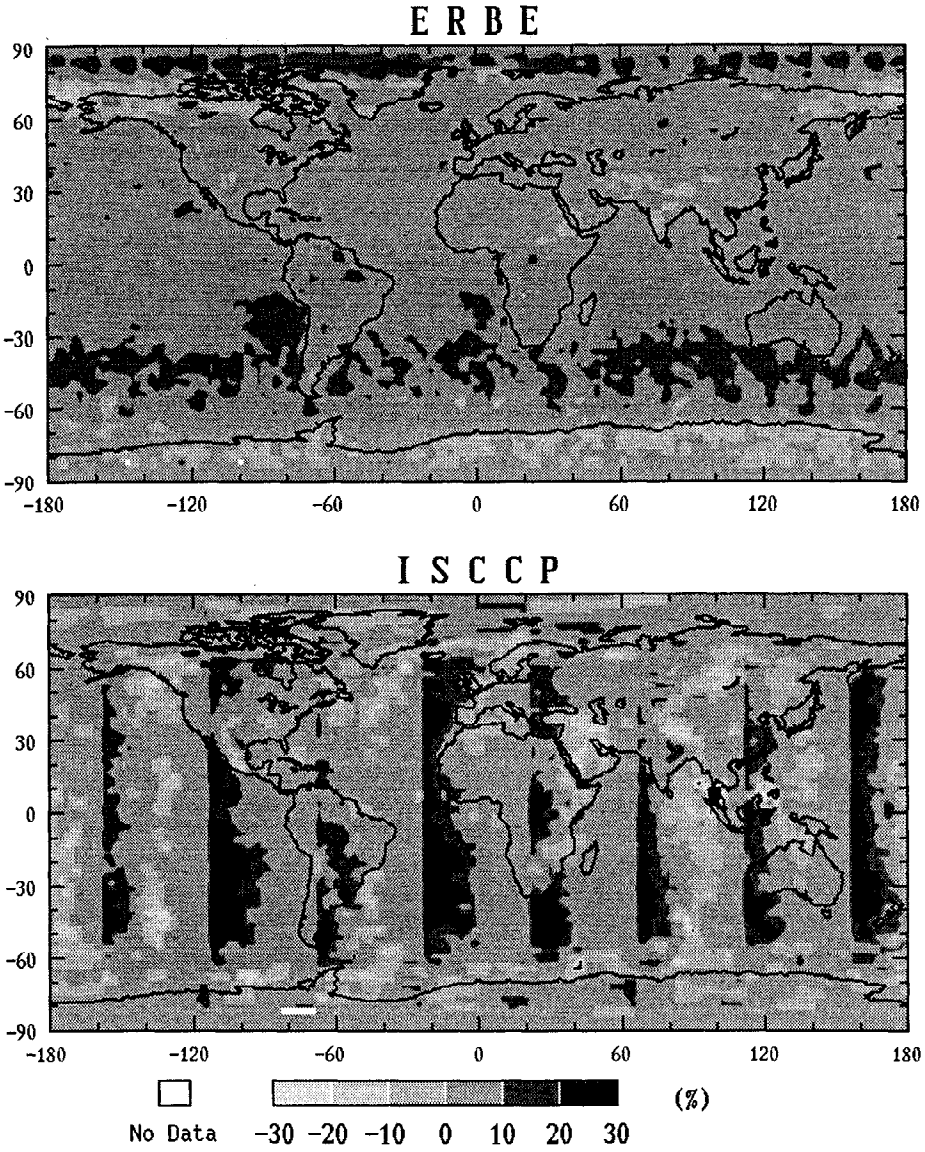

Figure 13. Global distribution of total albedo differences (0900 minus 1500 local time) for (top) ERBE and (bottom) ISCCP for April 1985.

that statistically significant values are found over large portions of land and thus the land/ocean contrast in the diurnal variation of LW CRF is true. However, we also see two interesting features from this pattern. First, the statistically significant values are seen over polar regions. This would simply indicate that although the diurnal variations of LW CRF over polar regions are small, the present test successfully captures it. Second, the statistical significance also occurs over the longitudinal belt from about 60°E to about 77°E over the Indian Ocean. The possible explanation for this feature is that the diurnal range of the ISCCP LW CRF might be relatively overestimated because of the inadequate diurnal sampling. The ISCCP data over this region have been provided by the Sun-synchronous NOAA 9 satellite that observes only twice a day in the tropics and midlatitudes. Consequently, this region has relatively lower measurements as shown in Figure 17, and thus the synoptic variability could bias the monthly statistics. The similar patterns are evident over the same region for the diurnal variations in cloud amount and the surface temperature minus cloud top temperature (Figure 7). Note that these spurious patterns in Figures 6 (bottom), 7, and 16 precisely occur in the area observed by NOAA 9 (Figure 17). It is therefore suggested that caution should be exercised when the ISCCP data are analyzed for the diurnal variations over regions where only a few observations a day are made.

4. Summary and Conclusions

In the present study we have presented the results of the diurnal variations of CRF in terms of four variables: monthly mean, diurnal range, time of maximum, and time of minimum. Although the ERBE and the ISCCP flux data exhibit fairly reasonable cloud structure in the global distribution of the monthly mean CRF, some differences are found in both LW and SW components. For the LW component, large differences occur in persistent cloud regions, such as the tropical convergence zone, where the significant biases of

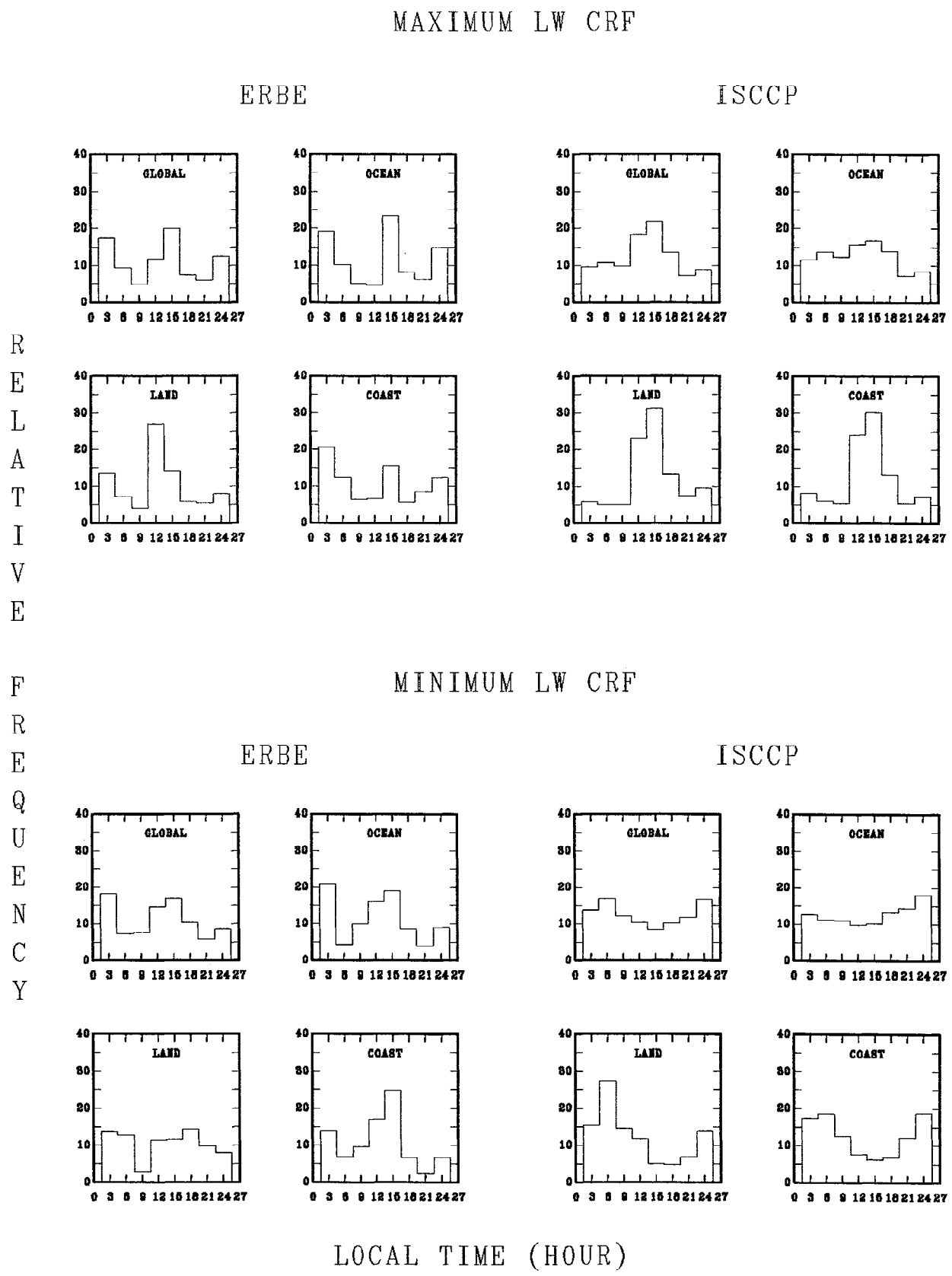

Figure 14. Times of (top) maximum and (bottom) minimum LW CRF histograms for four-month (April, July, and October 1985 and January 1986) averages. The *y* axis is given in percent.

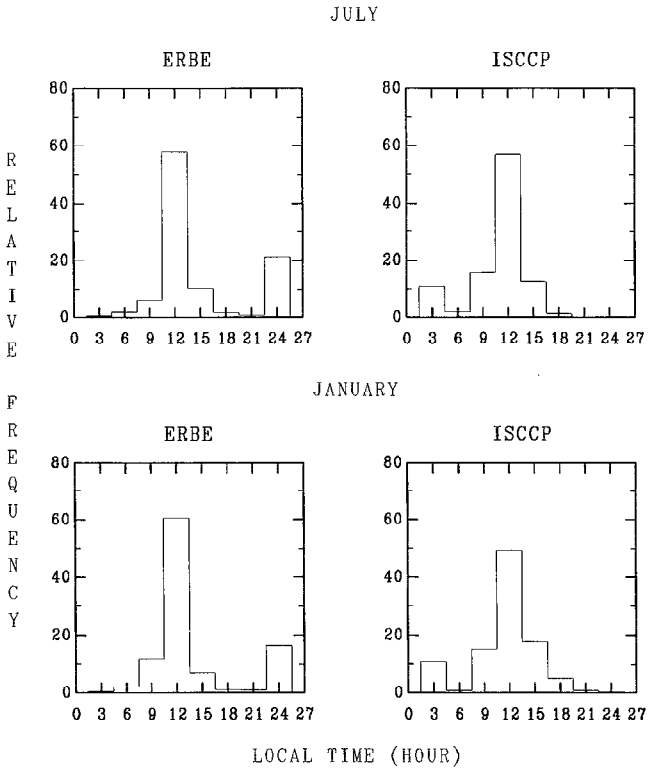

Figure 15. Times of maximum SW CRF histograms (global data) for July 1985 and January 1986. The y axis is given in percent.

clear-sky LW fluxes are seen to be responsible for these differences. Further studies may be needed to understand such clear-sky flux biases, even though we suggest two aspects concerning this problem: the ERBE scene identification problem and the ISCCP flux uncertainties caused by input data errors. For the SW component the ISCCP values are in general stronger than the ERBE estimates, except for the high NH latitudes where negative biases are shown to be related to scene identification difficulties over snow- and ice-covered regions.

The results of the diurnal range of LW CRF demonstrate two main features that are commonly present in both data sets. First, the land/ocean contrast is prominent in the global distribution of the LW CRF diurnal range. This contrast is shown to be associated with the land/ocean differences in the diurnal variations of cloud amount and the temperature difference between surface and cloud top. Furthermore, we have demonstrated that the large variabilities of LW CRF over land could be caused by clear-sky flux (i.e., surface temperature) variabilities. Second, both data sets generally show that the maximum diurnal range is found to be in the summer hemisphere and the minimum values in the winter hemisphere. These seasonal variations are also linked to the corresponding changes of cloud amount and the temperature difference between surface and cloud top as shown in Table 2. In addition, we note that the ISCCP data collected from polar orbiter measurements should be examined carefully for the analysis of diurnal variations, particularly over regions where only a few observations a day are available. Despite

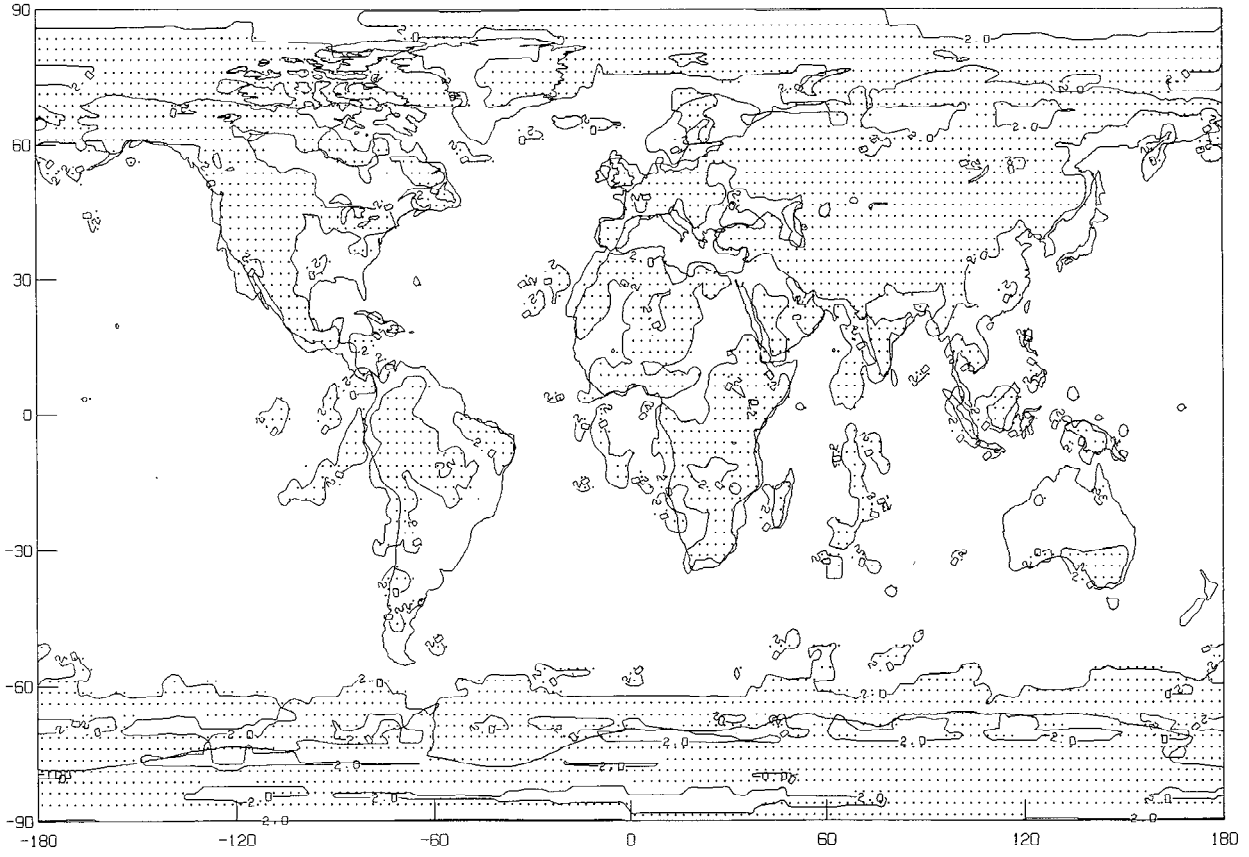

Figure 16. Fisher F distribution of the ISCCP LW CRF for April 1985. Areas with $F > 2$ (about at 95% statistical significance level) are stippled.

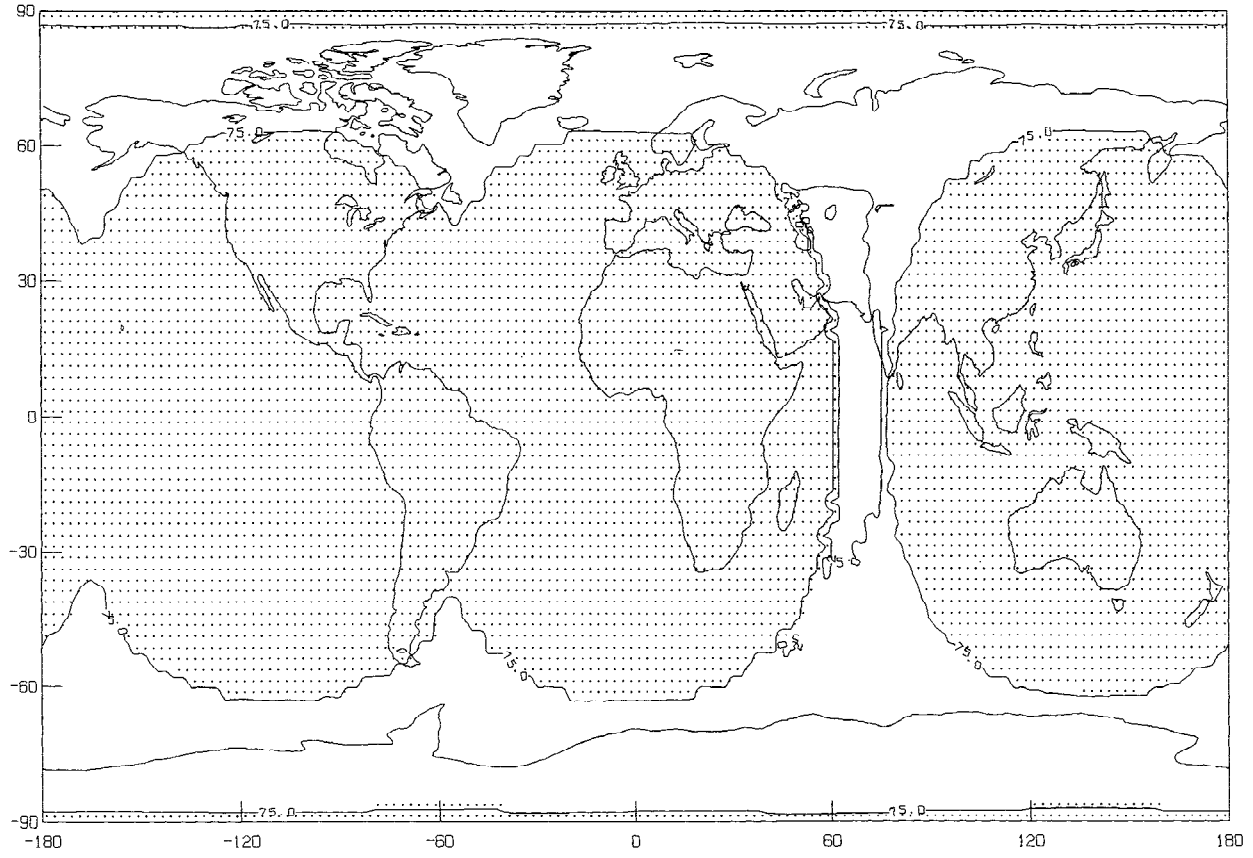

Figure 17. Relative frequency (percent) of the ISCCP satellite measurements for April 1985. Contours are at 25% and 75%.

the fact that the monthly mean LW CRF for ERBE is higher than the ISCCP value, the ERBE data underestimate the diurnal range of LW CRF. This is essentially because the ERBE diurnal sampling size is smaller than the ISCCP measurements, and thus the ERBE data do not capture the maximum and minimum values properly. The largest differences between two data sets, as consistent with the results of monthly mean differences, tend to occur in tropical convergence zones.

With respect to the times of maximum and minimum LW CRF, despite the large differences between two data sets on local and regional scales, both data sets show an overall agreement in that the daytime maximum and the nighttime minimum of LW CRF are observed over large portions of land and any time of the day over most oceans. For the SW CRF the maximum values during the day are about twice as large as monthly mean values, and their highest frequency occurs at local noon, indicating that solar insolation is a primary factor for the diurnal variation of SW CRF.

Acknowledgments. This work was accomplished while the author held the Columbia University/NASA Goddard Institute for Space Studies Postdoctoral Research Associateship, which was supported by the Department of Energy ARM program and the National Aeronautics and Space Administration through the ERBE project. I wish to thank B. Carlson and A. Lacis for their careful reviews of the manuscript and S. Doiron for programming assistance. I thank Y. Zhang and W. Rossow for providing the ISCCP flux data and for their helpful discussions and suggestions. I also appreciate numerous suggestions by two anonymous reviewers.

References

Albright, M. D., E. E. Recker, R. J. Reed, and R. Dang, The diurnal variation of deep convection and inferred precipitation in the central tropical Pacific during January–February 1979, *Mon. Weather Rev.*, *113*, 1663–1680, 1985.

Brooks, D. R., and P. Minnis, Simulation of the Earth's monthly average regional radiation balance derived from satellite measurements, *J. Clim. Appl. Meteorol.*, *23*, 392–403, 1984.

Brooks, D. R., E. F. Harrison, P. Minnis, J. T. Suttles, and R. S. Kandel, Development of algorithms for understanding the temporal and spatial variability of the Earth's radiation balance, *Rev. Geophys.*, *24*, 422–438, 1986.

Cess, R. D., and G. L. Potter, Exploratory studies of cloud radiative forcing with a general circulation model, *Tellus*, *39*(A), 460–473, 1987.

Charlock, T. P., and V. Ramanathan, The albedo field and cloud radiative forcing produced by a general circulation model with internally generated cloud optics, *J. Atmos. Sci.*, *42*, 1408–1429, 1985.

Cheruy, F., R. S. Kandel, and J. P. Duvel, Outgoing longwave radiation and its diurnal variations from combined Earth Radiation Budget Experiment and Meteosat observations, 2, Using Meteosat data to determine the longwave diurnal cycle, *J. Geophys. Res.*, *96*, 22,623–22,630, 1991.

Duvel, J. P., Convection over tropical Africa and the Atlantic Ocean during northern summer, I, Interannual and diurnal variations, *Mon. Weather Rev.*, *117*, 2782–2799, 1989.

Fu, R., A. D. Del Genio, and W. B. Rossow, Behavior of deep convective clouds in the tropical Pacific deduced from ISCCP radiances, *J. Clim.*, *3*, 1129–1152, 1990.

Gray, W. M., and R. W. Jacobson, Jr., Diurnal variation of deep cumulus convection, *Mon. Weather Rev.*, *105*, 1171–1188, 1977.

Hansen, J., G. Russell, D. Rind, P. Stone, A. Lacis, S. Lebedeff, R. Ruedy, and L. Travis, Efficient three-dimensional global models

for climate studies: Models I and II, *Mon. Weather Rev., 111*, 609–662, 1983.

Harrison, E. F., et al., First estimates of the diurnal variation of longwave radiation from the multiple-satellite Earth Radiation Budget Experiment (ERBE), *Bull. Am. Meteorol. Soc., 69*, 1144–1151, 1988.

Harrison, E. F., P. Minnis, B. R. Barkstrom, V. Ramanathan, R. D. Cess, and G. G. Gibson, Seasonal variation of cloud radiative forcing derived from the Earth Radiation Budget Experiment, *J. Geophys. Res., 95*, 18,687–18,703, 1990.

Hartmann, D. L., and D. Doelling, On the net radiative effectiveness of clouds, *J. Geophys. Res., 96*, 869–891, 1991.

Hartmann, D. L., K. J. Kowalewsky, and M. L. Michelsen, Diurnal variations of outgoing longwave radiation and albedo from ERBE scanner data, *J. Clim., 4*, 598–617, 1991.

Kandel, R., Satellite observation of the Earth radiation budget, *Beitr. Phys. Atmos., 56*, 322–340, 1983.

Karl, T. R., P. D. Jones, R. W. Knight, G. Kukla, N. Plummer, V. Razuvayev, K. P. Gallo, J. Lindseay, R. J. Charlson, and T. C. Peterson, A new perspective on recent global warming: Asymmetric trends of daily maximum and minimum temperature, *Bull. Am. Meteorol. Soc., 74*, 1007–1023, 1993.

Kyle, H. L., R. R. Hucek, and B. J. Vallette, Atlas of the Earth's radiation budget as measured by Nimbus-7: May 1979 to May 1980, *NASA Ref. Publ., 1263*, 133 pp., 1991.

Ramanathan, V., R. D. Cess, E. F. Harrison, P. Minnis, B. R. Barkstrom, E. Ahmad, and D. Hartmann, Cloud-radiative forcing and climate: Results from the Earth Radiation Budget Experiment, *Science, 243*, 57–63, 1989.

Rieland, M., and E. Raschke, Diurnal variability of the Earth radiation budget: Sampling requirements, time integration aspects and error estimates for the Earth Radiation Budget Experiment (ERBE), *Theor. Appl. Climatol., 44*, 9–24, 1991.

Rossow, W. B., and R. A. Schiffer, ISCCP cloud data products, *Bull. Am. Meteorol. Soc., 72*, 2–20, 1991.

Rossow, W. B., A. W. Walker, and L. C. Garder, Comparison of ISCCP and other cloud amounts, *J. Clim., 6*, 2394–2418, 1993.

Stephens, G. L., and T. J. Greenwald, The Earth's radiation budget and its relation to atmospheric hydrology, 1, Observations of the clear sky greenhouse effect, *J. Geophys. Res., 96*, 15,311–15,324, 1991.

Y. Kim, NASA Goddard Institute for Space Studies, 2880 Broadway, New York, NY 10025.

(Received October 20, 1993; revised June 6, 1994;
accepted June 27, 1994.)